Forestry An International Journal of Forest Research

Institute of Chartered Foresters

Forestry 2020; **93**, 411–429, doi:10.1093/forestry/cpz067
Advance Access publication 2 January 2020

Original article

Estimating tree stem diameters and volume from smartphone photogrammetric point clouds

Maria Immacolata Marzulli[1,*], Pasi Raumonen[2], Roberto Greco[1], Manuela Persia[1] and Patrizia Tartarino[1]

[1]*Department of Agricultural and Environmental Sciences, University of Bari A. Moro, Via Amendola 165/A, 70126 Bari, Italy*
[2]*Mathematics, Tampere University, Korkeakoulunkatu 7, 33720 Tampere, Finland*

* Corresponding author Tel: +(39)0805443024; E-mail: maria.marzulli@uniba.it

Received 4 October 2018

Methods for the three-dimensional (3D) reconstruction of forest trees have been suggested for data from active and passive sensors. Laser scanner technologies have become popular in the last few years, despite their high costs. Since the improvements in photogrammetric algorithms (e.g. structure from motion—SfM), photographs have become a new low-cost source of 3D point clouds. In this study, we use images captured by a smartphone camera to calculate dense point clouds of a forest plot using SfM. Eighteen point clouds were produced by changing the densification parameters (Image scale, Point density, Minimum number of matches) in order to investigate their influence on the quality of the point clouds produced. In order to estimate diameter at breast height (d.b.h.) and stem volumes, we developed an automatic method that extracts the stems from the point cloud and then models them with cylinders. The results show that Image scale is the most influential parameter in terms of identifying and extracting trees from the point clouds. The best performance with cylinder modelling from point clouds compared to field data had an RMSE of 1.9 cm and 0.094 m^3, for d.b.h. and volume, respectively. Thus, for forest management and planning purposes, it is possible to use our photogrammetric and modelling methods to measure d.b.h., stem volume and possibly other forest inventory metrics, rapidly and without felling trees. The proposed methodology significantly reduces working time in the field, using 'non-professional' instruments and automating estimates of dendrometric parameters.

Introduction

Traditionally, foresters use mechanical or optical instruments, such as calipers, hypsometers and measuring tapes, to measure biometric parameters in field plots. These traditional methods are time-consuming and cannot directly measure some tree attributes, such as stem volume and biomass components (total, stem and branches). Assessing the later parameters in the field typically requires felling the trees (Liang *et al.*, 2016) or relying on allometries of earlier studies that felled and measured trees to establish these allometries. Numerous studies applied mathematical functions for representing the longitudinal profile of stems of certain species. These equations were used to estimate the diameters of cross sections of the stem at different heights from the ground, and the volume of stem portions, or to represent the particular shape of the stem (Brink and Gadow, 1986; Tarp-Johansen *et al.*, 1997; Gaffrey *et al.*, 1998; Dhôte *et al.*, 2000; Kublin, 2003). These functions are useful for describing the stem profile at varying heights from the ground. However, this type of approach does not consider the particular morphology and inclination of individual stems, which are difficult parameters to evaluate on standing trees.

In the last two decades, introduction of terrestrial laser scanning (TLS) technologies has increased the set of available methods for assessing forest attributes in the field (Moskal and Zheng, 2011; Kankare *et al.*, 2015; Liang *et al.*, 2016; Giannetti *et al.*, 2018). There is growing interest in using TLS to estimate biometric parameters of trees, based on their three-dimensional (3D) reconstruction. The 3D reconstruction of trees does not only enable estimating d.b.h. (Maas *et al.*, 2008; Strahler *et al.*, 2008; Huang *et al.*, 2011; Liang *et al.*, 2014) and volume (Liang *et al.*, 2014) but also possible to measure other biometric parameters useful for forest management and planning purposes including biomass (Van Aardt *et al.*, 2008) and stem locations. Furthermore, some metrics that have less frequently been addressed so far, including lower crown height, or crown depth may potentially be extracted. The latter could be estimated by combining point clouds collected from the ground and from the air.

The reconstruction of trees from 3D point clouds has been mostly accomplished using cylinder fitting algorithms so far. Although the cross sections of tree stems are generally ellipsoidal, the ratio between the major and the minor axes of these ellipses is close to 1 (Patrone, 1963), particularly if they are not located on heavily sloping lands or in areas subject to strong dominant winds. Therefore, since the diameters do not change very quickly along the stem, the use of cylinders enables good estimates of the volume on a relatively short vertical section (Åkerblom *et al.*, 2015). Corresponding approaches were for example presented in the work of Dassot *et al.* (2012), Hackenberg *et al.* (2014), Calders *et al.* (2015), Hackenberg *et al.* (2015) and Stovall and Shugart (2018).

There is an ongoing discussion whether the efficiency of forest inventories could be improved using TLS in combination with automatic procedures extracting the desired tree metrics (Liang *et al.*, 2016; Giannetti *et al.*, 2018). Besides a potential improvement in efficiency, TLS data provide a permanent detailed spatial record of the forest structure of a given area. It could thus be possible to carry out temporal monitoring of measured parameters through additional acquisitions over time (Liang *et al.*, 2012; Srinivasan *et al.*, 2014; Liang *et al.*, 2016).

However, TLS data acquisition is limited by the time and costs involved (Mikita *et al.*, 2016; Wilkes *et al.*, 2017), limited software and a possible lack of trained personnel (Liang *et al.*, 2016). The mobility of instruments is still relatively low and hardware costs, although decreasing, are still rather high (Giannetti *et al.*, 2018).

Considering particularly the latter points, photogrammetric approaches may be an interesting alternative to TLS based approaches. Given the improvements in photogrammetric algorithms, image-based techniques are now able to produce 3D point cloud data that are similar to the data obtained with TLS technologies (Cavegn *et al.*, 2014; Liang *et al.*, 2015; Liang *et al.*, 2016). The most commonly applied algorithm is structure from motion (SfM) (Ullman, 1979; Szeliski, 2011). Similar to traditional photogrammetry, SfM uses images acquired from multiple viewpoints and dense image-matching algorithms, such as the Scale Invariant Feature Transform (SIFT) (Lowe, 2004) and the Speeded-Up Robust Features (SURF) (Bay *et al.*, 2008), to create the 3D geometry of an object or surface present in multiple images (Remondino and Fraser, 2006; Remondino *et al.*, 2012; Verhoeven *et al.*, 2013; Wallace *et al.*, 2016; Bakker and Lane, 2017).

Several studies have demonstrated the feasibility of using terrestrial images as a source of point cloud data for tree mapping (Morgenroth and Gomez, 2014; Liang *et al.*, 2015; Miller *et al.*, 2015; Forsman *et al.*, 2016; Mikita *et al.*, 2016; Panagiotidis *et al.*, 2016; Surový *et al.*, 2016) and as a low-cost alternative to TLS (Liang *et al.*, 2014). The main advantage of image-based techniques is that they produce similar outputs to TLS systems, but use less expensive hardware (Mokroš *et al.*, 2018), i.e. small and light instruments that are affordable and easy for non-professional users to operate. As stated by Liang *et al.* (2016), in the future, an untrained person may be capable of carrying out forest inventories using photogrammetry after a short instruction. This method could therefore significantly reduce the cost of field plot inventories, thus increasing the number of field plots and enhancing forest field inventories (Liang *et al.*, 2016).

Approaches to collect image-based point clouds in forestry applications vary in terms of the image acquisition system and accuracy assessment of the point cloud obtained. The image acquisition phase is very important. Mokroš *et al.* (2018) present seven data collection methods, which differ in terms of camera orientation, shooting mode and photographic path. These authors found that the most accurate method used vertical camera orientation, stop-and-go walking rhythms and a path around the plot with two diagonal paths through the plot. Liang *et al.* (2015) proposed an application of terrestrial image-based point clouds acquired with a handheld camera for forest plot inventories. They used two photographic paths to take photos: a circular path inside the plot (30 × 30 m) with the camera pointing out of the plot and a closed loop outside the plot. Panagiotidis *et al.* (2016) took 350 photos in a circular plot with a 6 m radius, following the photographic path along the perimeter of the plot and pointing the camera at eye level, at the base and at the top of the tree. Mikita *et al.* (2016) used aerial and terrestrial images to obtain a dense point cloud of a 0.8 ha research plot. The terrestrial images were captured by walking through the forest at 5 km h^{-1}, with one captured image per second. Forsman *et al.* (2016) developed a method for terrestrial mapping of tree structures; they used a multi-camera rig with five cameras, taking all images from the centre of the field plot, looking outwards in different directions. Piermattei *et al.* (2019) estimated diameter at breast height (d.b.h.) and stem curves up to 2.8 m above the ground using a cylinder fitting method in four forest plots with a tree density ranging from 390 to 875 stems ha^{-1}.

In most cases, the accuracy of the reconstructed 3D models was assessed by comparing the d.b.h. and heights measured in the field with those obtained using the 3D model and analysing the root mean square error (RMSE) or percentage error values for each parameter (Liang *et al.*, 2014; Morgenroth and Gomez, 2014; Liang *et al.*, 2015; Mikita *et al.*, 2016; Surový *et al.*, 2016). In Panagiotidis *et al.* (2016), forest inventory metrics (d.b.h. and height) obtained from the terrestrial photogrammetry point clouds were compared with those measured on the TLS point clouds.

In this study, we build upon the findings of these earlier studies but examine several new aspects. First, we derived our 3D point clouds from images taken with a smartphone camera, which has rarely been examined so far. Considering a future operationalization of the presented approach, we developed and tested an image acquisition grid (walking pattern) that fits most practical cases. This is an important step to standardize the image acquisition phase. Further, we tested the influence of the different densification parameters (Image scale, Point density, Minimum number of matches) in the SfM algorithm to produce the point clouds to analyse which kind of set-up leads to the best results. Finally, we also developed an automatic cylinder fitting method to extract and model individual tree stems from the image-based point clouds. Although cylinder stem modelling has been applied to TLS point clouds, to our knowledge there were no previous applications on image-based data. Therefore, the overall aim of this study was to estimate the accuracy and feasibility of using SfM and cylinder stem modelling techniques for d.b.h. and volume estimates of forest stands.

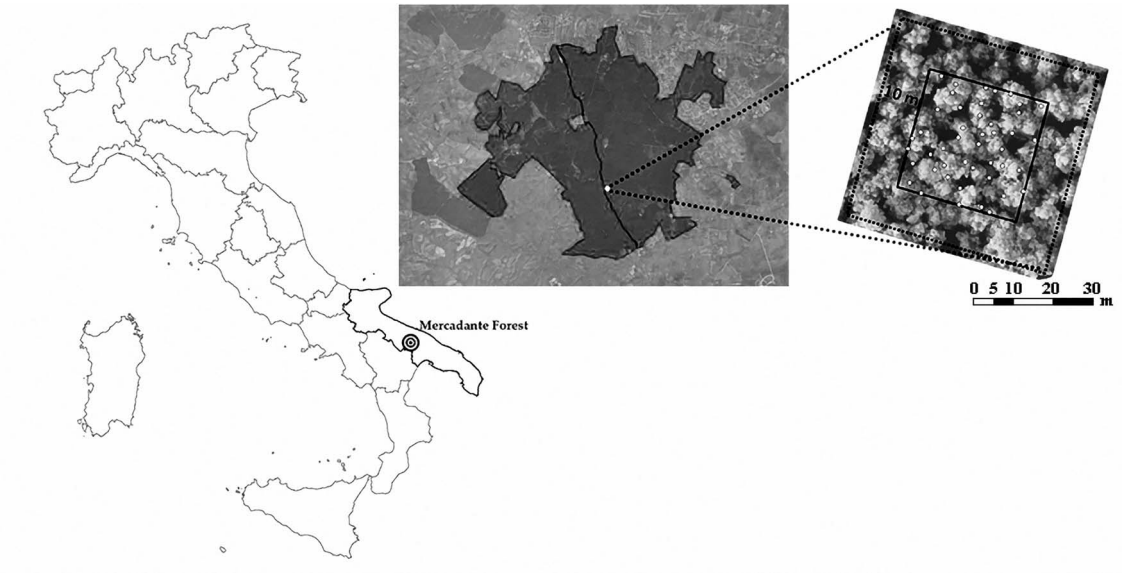

Figure 1 Location of the forest plot in Mercadante Forest within Italy.

Materials and methods

Study area

The forest plot used in our study is located in Puglia, southern Italy (Figure 1). It is part of the Mercadante Forest (1300 ha) in the Alta Murgia National Park. The forest was created by hydrogeological afforestation work to counteract the descent of rainwater from the Murgia uplands after floods struck the Bari area in the early 1900s. The plot is characterized by an even-aged forest stand, and the main tree species are Aleppo pine (*Pinus halepensis*) and cypress (*Cupressus sempervirens*). The plot (Figure 1) is 30 × 30 m with a buffer zone of 10 m around the plot to enable photographic surveys. It consists of 45 trees (∼500 stems ha^{-1}) and was chosen for the scarce presence of undergrowth combined with a good density of arboreal vegetation.

Dendrometric parameters measured in the field

D.b.h. (measured at 1.30 m above ground level) and species were recorded in the field. A caliper was used to measure d.b.h. as the average of two perpendicular diameters. The 45 trees in the plot had a mean d.b.h. of 28.90 cm (max = 49.70 cm, min = 15.70 cm).

Starting from the base of the trees, diameters were measured every 1 m using Wheeler's pentaprism integrated with a hypsometer to estimate the volume of the standing tree stems. These measurements were taken for 15 'volume model trees' out of the total of 45 trees, which were randomly selected among the most visible trees. Upper stem diameters were measured up to a height of 12 m, but for some trees it was limited to 6 m. At higher heights, it became increasingly difficult to measure stem diameters as the visibility in the pentaprism decreased. Hence, volumes by section were estimated up to a height of 6 m. Tree heights of the volume model trees were measured by a Häglof VL5 Vertex Laser hypsometer (max = 20.6 m, min = 12 m, mean = 17.80 m).

Volume estimates in the field

Diameters measured at different heights in the field enabled the areas of tree cross sections to be calculated at each height. The volume of each tree stem portion was calculated using Smalian's formula (Loetsch *et al.*, 1973):

$$V' = \left(\frac{S_1 + S_2}{2}\right) \bullet h, \quad (1)$$

where S_1 and S_2 are the areas of the two last sections of the stem portion, and h is the height of each stem section, which was selected as equal to 1 m. The data from field measurements were compared with those obtained using cylinder modelling.

Terrestrial photogrammetry

Images were taken on the same day using a smartphone camera with a focal length of 28 mm (35 mm equivalent) and a lens aperture of f/1.9. The ISO sensitivity of the camera was set to 80 and the exposure time to 1/250 s, which matched the local light conditions. The smartphone used was a Samsung Galaxy S6 and it was mounted on a DJI OSMO Mobile smartphone stabilizer.

A total of 686 photos were taken using the stop-and-go method and following the photographic path shown in Figure 2. The images were captured at a distance of 2.5 m from each other and at two different height levels (2 and 4 m above ground), using a telescopic bar. The choice of the image acquisition grid was based on our experience with previous surveys and aimed to optimize the percentage overlap between the images. Photos were taken in different light conditions due to the position of the sun in relation to the study plot. Light conditions were optimal in the forward survey images, unlike those in the return survey, which were taken under backlighting conditions, with the camera pointed at the sun. Image resolution was 5312 × 2988 pixels. It took ∼30 min to acquire the photos on a single path, and a total of ∼3 h to complete the full photographic survey.

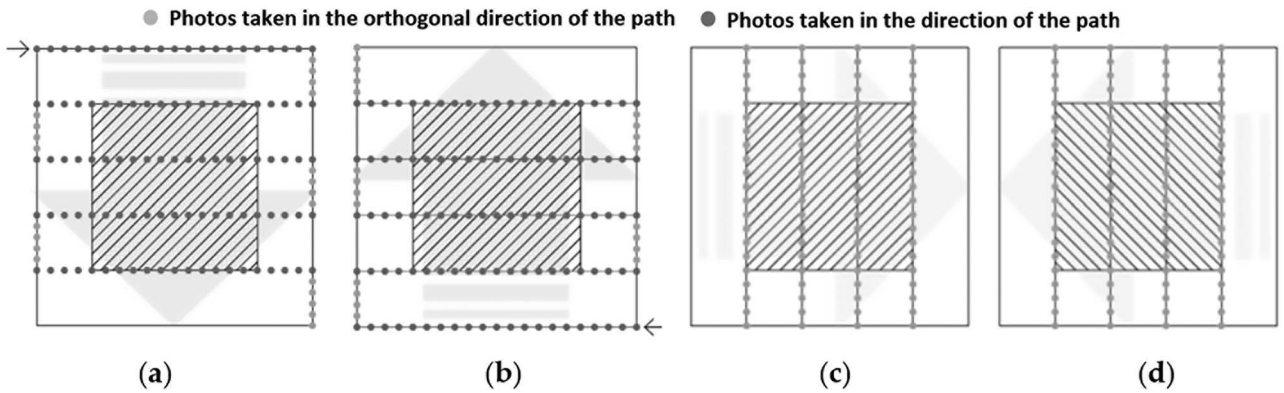

Figure 2 (a) Path of the forward photographic survey; (b) path of the return photographic survey; (c, d) path of the lateral photographic survey. The large arrows in the images show the direction of progress of the survey.

In addition, in order to allow scaling and georeferencing of the 3D point clouds obtained with SfM processing, a Trimble PROXH GPS receiver was used to collect the GPS coordinates of five ground control points (GCPs) that were well distributed in the plot area. Five black and yellow squared targets (20 × 20 cm) were used to identify the positions of the five GCPs in the images in which they were visible.

Data processing

The images captured in the terrestrial survey were processed using Pix4Dmapper (Pix4D SA). This software implements a fully automated photogrammetric workflow for indoor, terrestrial, oblique and nadir imagery. Detailed descriptions of the Pix4D workflow can be found in the study of Küng et al. (2011).

Data were processed using a 64-bit system with an Intel Core i7-7700 CPU at 3.6 GHz, 6 GB GPU and 64.0 GB RAM, and the process took ~1 h for each point cloud produced.

We tested the influence of the following parameters on the resulting point cloud densification:

- Image scale (1, 1/2, 1/4, 1/8), which defines the scale of the images at which additional 3D points are computed.
- Point density, which defines the density of the densified point cloud. If set to optimal, a 3D point is computed for every [4/Image scale] pixel; if set to high, a 3D point is computed for every [Image scale] pixel; if set to low, a 3D point is computed for every [16/Image scale] pixel. It is also strongly affected by the previously set Image scale.
- Minimum number of matches, which represents the minimum number of valid reprojections of each 3D point to the images. This can range from 3 to 6.

The software default parameters are 1/2 Image scale, Optimal point density and 3 as the Minimum number of matches. Varying the parameters resulted in different numbers of 3D points and average densities (per m^3).

In total, 18 point clouds were produced, combining the parameters only in combinations which resulted in sufficiently dense point clouds (Table 1).

Table 1 Densification parameters for the point clouds.

Index	Image scale	Point density	Minimum no. of matches	No. of 3D densified points	Average density (per m^3)
1	1/8	High	3	2 261 079	660
2	1/8	Optimal	3	546 487	255
3	1/8	Low	3	138 122	109
4	1/4	High	3	7 204 110	2028
5	1/4	High	4	4 568 156	1624
6	1/4	High	5	2 741 030	1243
7	1/4	Optimal	3	2 058 359	697
8	1/4	Optimal	4	1 267 541	532
9	1/4	Optimal	5	904 610	386
10	1/4	Low	3	536 909	247
11	1/2	High	4	18 013 134	4352
12	1/2	High	5	10 986 920	3331
13	1/2	High	6	6 557 732	2467
14	1/2	Optimal	3	13 154 154	1232
15	1/2[1]	Optimal	3	3 736 455	1492
16	1/2	Optimal	4	5 127 568	1388
17	1/2	Optimal	5	3 040 808	1035
18	1/2	Low	3	2 260 114	602

[1]This point cloud has been unchecked the option 'Multiscale' (additional 3D points are computed on multiple image scales, starting with the chosen scale and going to the 1/8 scale).

Point cloud processing

Before the identification and modelling of the tree stems, the plot point cloud produced by photogrammetry was filtered (Figure 3) to remove non-tree points, such as points from the ground, understory and noise (incorrectly identified points).

This process contains five steps. First the point cloud was clipped to the area of interest to exclude areas outside the plot. Then, it was downsampled by partitioning the space containing the point cloud into small cubes (voxels—here we used 1 cm edge length) and keeping only one point from each non-empty cube

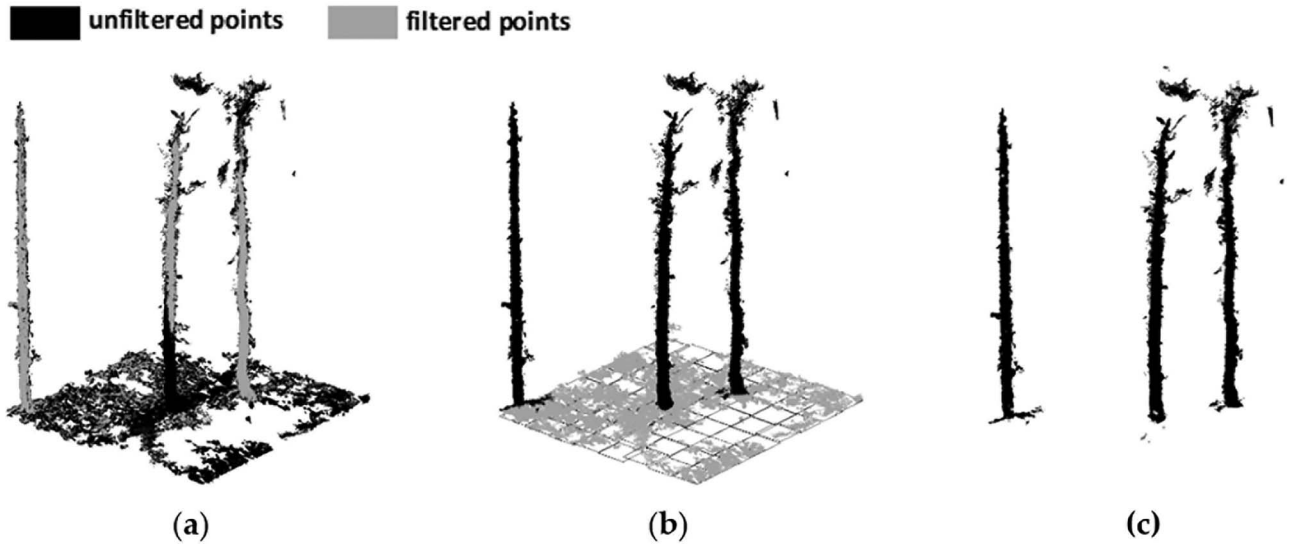

Figure 3 Filtering steps for point clouds. Grey points are filtered out. (a) Downsampling, (b) approximation of ground level (rectangles) and removing points near ground and (c) noise filtering based on point density.

(Figure 3a). Next, the ground level was approximated as a grid of horizontal squares covering the point cloud. The edge length of the squares was 1 m. The height of the squares was the height (z-coordinate) of the lowest point inside the squares (Figure 3b). Then, based on this ground level model, all points below a height of 20 cm were removed, and points up to a height of 2 m were removed if the third meter above ground level contained no points (Figure 3b). Finally, some noise was filtered out based on local point densities: for this, the space was divided into cubes measuring 5 × 5 × 5 cm, and the points were kept inside a cube if there were at least five points (for some very low-density point clouds, thresholds below five were used; Figure 3c).

Stem extraction and cylinder modelling from point clouds

In this section, we describe how the stems were extracted from the point cloud and how they were modelled with two different cylinder models. Figure 4 shows the workflow of this process, and the details are given in the following subsections.

Covering the point cloud with patches

Potential stem sections are considered to be large vertically continuous subsets of the point cloud above the ground level. To extract them, firstly the point cloud was covered with surface patches, which are small subsets of the point cloud. These patches were used as the smallest 'units' or 'building blocks' for segmenting the point cloud into stems. Their location and diameter (between 10 and 20 cm) were randomly generated as the branching structures of the trees were, at this stage of the methodology, still unknown. Also, the neighbours of the patches were identified and used for region growing. The patch generation process is explained in the study of Raumonen *et al.* (2013). Figure 5a shows examples of the surface patches.

Locating potential stem sections

Then, based on the height of the patches, layers of the patches were iteratively processed from the highest to the lowest layer: all patches between 2.5–4.0, 2.0–3.5, 1.5–3.0, 1.0–2.0 and 0.3–1.0 m above the ground were iteratively selected (Figure 5a). For each layer, the connected components of the patches in the layer were identified: each component is the collection of all the patches that are connected to each other in the sense of the neighbour–relation of the patches. Each component that had more than 15 patches was a potential section containing a stem (Figure 5b). When all the potential stem sections from one iteration had been identified, they were processed one at a time, from the section containing the largest number of patches to the section containing the smallest number of patches, in order to see if they could be extended to the whole stem. When the stems from one layer had been identified, those stem points were no longer used in other layers for locating stems. In addition, potential stem sections were disregarded after expansion if they contained points from already identified stems.

Cylindrical surface coverage

The potential stem sections were processed to find the best possible stem subset from the point cloud. A subset is considered a real stem section based on how completely the surface of the section is covered with points or how high is the so-called cylindrical surface coverage. The cylindrical surface coverage was estimated using two lines, an axis line inside the stem section and another line orthogonal to it, as a reference for partitioning the points close to the line into subsets that were intersections of sectors and horizontal layers. A random reference direction orthogonal to the axis and a given point in the axis make it possible to compute a single angle and projected height for each point (see Figure 6a–c). Practical estimation of surface coverage was performed as follows: using an axis line in space (and a point in the line) and a random orthogonal direction as a reference, the

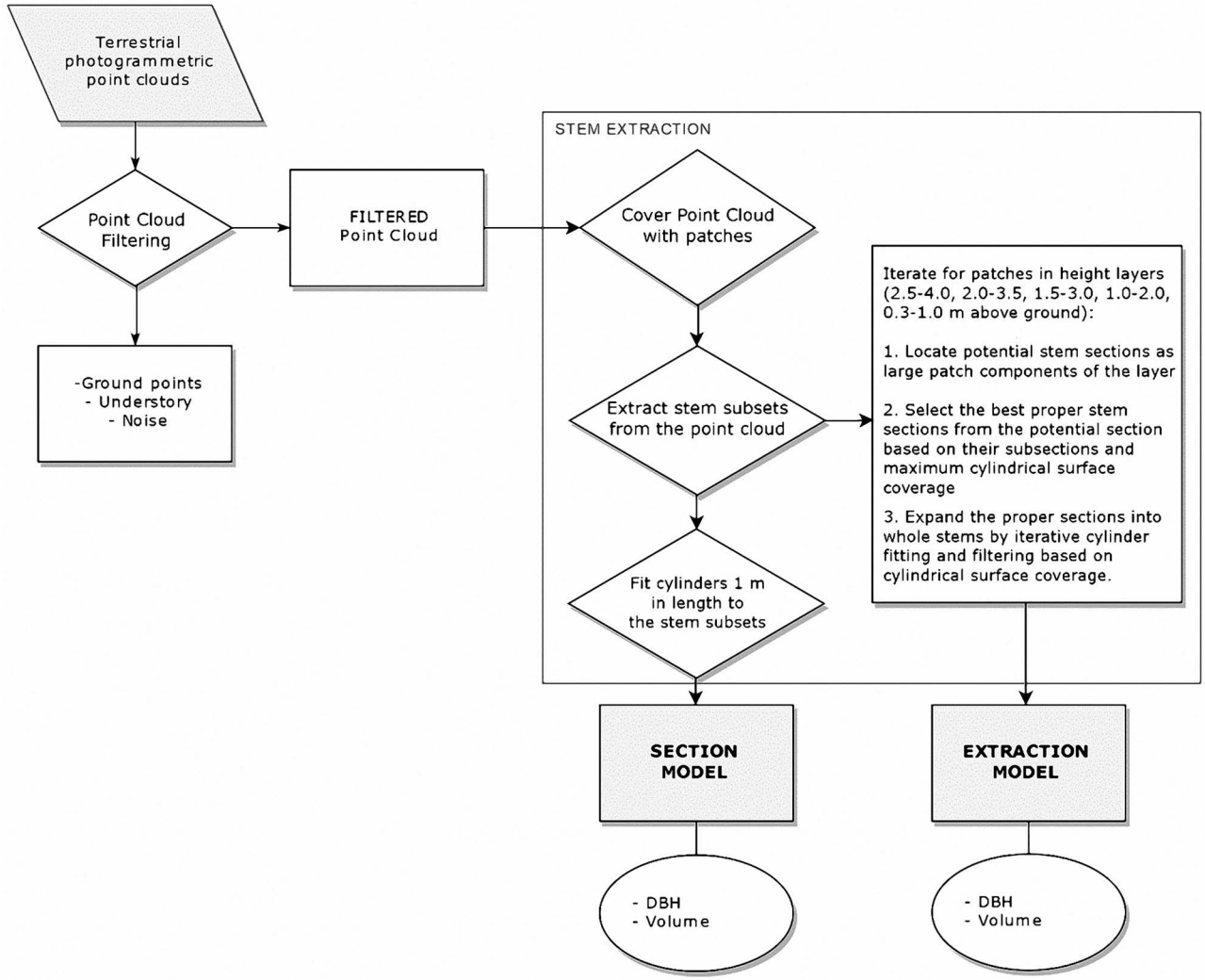

Figure 4 Workflow of the stem extraction and cylinder modelling.

points close to the line were divided into 20 equal-angle sectors and 10 equal-height layers. The intersection of these sectors and layers produced a partition of 200 subsets (see the example in Figure 6) and the relative number of non-empty subsets gave the surface coverage.

Selecting a proper stem section

In order to correctly select only one stem from multi-stem trees or sections containing points from two neighbouring stems, a potential stem section was first expanded with five layers of neighbours (patches outside the layer defining the section) and then divided into layers ∼30 cm high. With this step, the connected components of the layers were determined. Considering each component as a stem section, its axis line was estimated and applied to estimate the surface coverage on the whole expanded stem section. The axis line giving the highest surface coverage was then chosen to define the final stem section. The extended stem section was once again partitioned into 200 subsets as above, and the points closest to the axis were selected from each subset (Figure 6d). Then, a cylinder was fitted into this filtered section, and the cylinder was accepted if it was reasonable, i.e. a radius of <1 m, axis nearly vertical, and surface coverage over 40 per cent.

Expanding stem sections into full stems

Once a stem section had been defined, it was then expanded into the whole stem by first expanding it towards the ground and then upwards, as follows. The cylinder axis and radius were used to extract 3D subsets from the point cloud below the cylinder (or above it, when moving upwards), so that the length of the subset was increased iteratively and so that the distance of the points from the axis was less than three times the radius. The length of the subsections was increased from ∼3 times the radius up to ∼16 times the radius. The subsets were filtered according to the surface coverage, as above. They were then fitted with cylinders to estimate their axis and radius. The subset with the

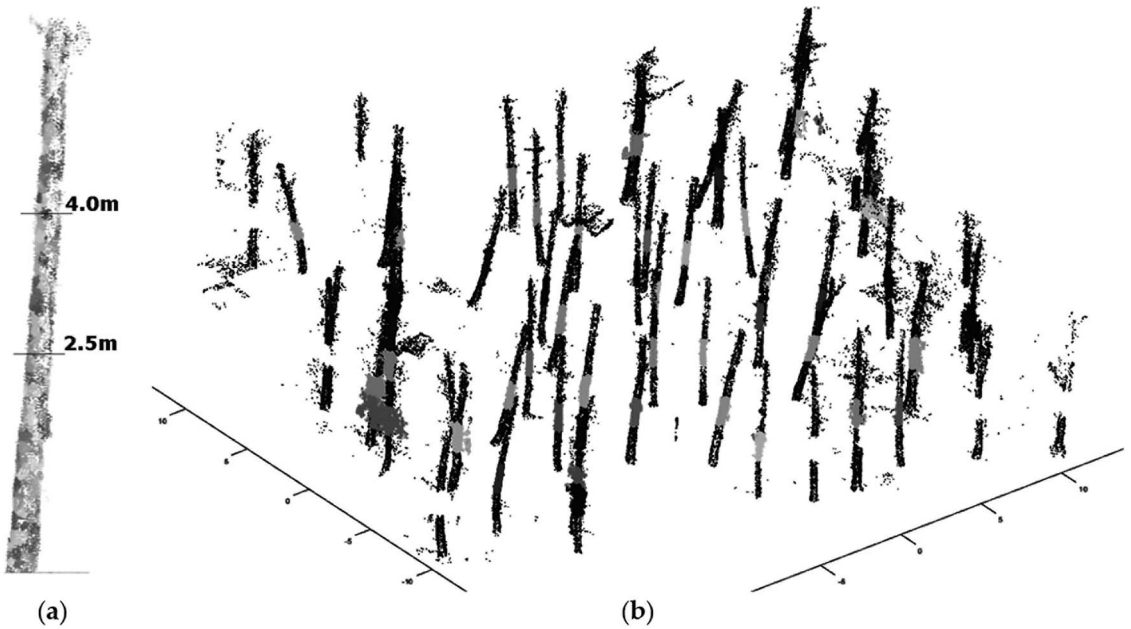

Figure 5 Locating potential stem segments. (a) Close-up of a stem point cloud portioned into patches and (b) different colours denote large enough patch components, which work as initial stem section candidates that are later expanded into full stems.

greatest surface coverage was selected as the one that continues the stem. This process was then repeated until the ground was reached. The process continued upwards as long as there were sufficient points (at least 20), and the axis and radius were similar to the cylinder below. The result of the process was a subset of the point cloud containing the stem and cylinders that model its surface.

Extraction Model and Section Model

The above process of extracting stem point clouds used cylinders and produced a cylinder model for each extracted stem. We call this the 'Extraction Model'. Subsequently, the stems were modelled again with cylinders, but now the locations and lengths of the cylinders were fixed for a comparison with the manual diameter measurements. First, a cylinder was fitted around a height of 1.3 m (section 1.0–1.6 m) to accurately estimate d.b.h.. Then, the entire stem was fitted with cylinders so that they covered the sections 0–0.5, 0.5–1.5, 1.5–2.5 m, etc. up to the top. Apart from the first mentioned, the midpoints of these cylinders were at a height of 1, 2, 3 m, etc., which were the same heights as the diameter measurements. The section volumes thus match the volume estimated from the diameter measurements using equation (1). We call this the 'Section Model'.

The surface patch generation needed in stem extraction has a random seed; therefore, when repeated, it always produces a different partition of the point cloud into patches. Thus, repeating the extraction process and cylinder modelling will always generate small variations and in some sensitive cases larger differences; for example, a stem may be found and extracted in one iteration but not in another. Extraction and cylinder modelling were repeated 10 times for each point cloud to capture the uncertainty in the process. The averages (i.e. volumes) from the 10 iterations were used as the result, and standard deviation estimates the uncertainty in the results.

Statistics to evaluate the modelling results

To evaluate our modelling results, we calculated the RMSE and bias as defined in equations (2) and (3):

$$\text{RMSE} = \sqrt{\frac{\sum_n (\text{estimated} - \text{measured})^2}{n_{\text{trees}}}} \quad (2)$$

$$\text{Bias} = \frac{\sum_n (\text{estimated} - \text{measured})}{n_{\text{trees}}} \quad (3)$$

In both formulas, estimated values were calculated as the average value of d.b.h. or volume from the 10 iterations for each tree. The percentage values of these parameters were obtained by comparing each one with the average measured value.

The uncertainty and accuracy of the modelling results were estimated by analysing the standard deviation and absolute error of d.b.h. and section volume for each tree of the 18 point clouds from the 10 iterations. Then for each point cloud, the mean standard deviation and mean absolute error values were calculated as the average value of the 45 single-tree standard deviations and absolute errors.

Results

Stem extraction and cylinder modelling from point clouds

Results obtained for each point cloud varied in the number of reconstructed trees and stems found in different iterations. Table 2 shows the number of trees found by applying our

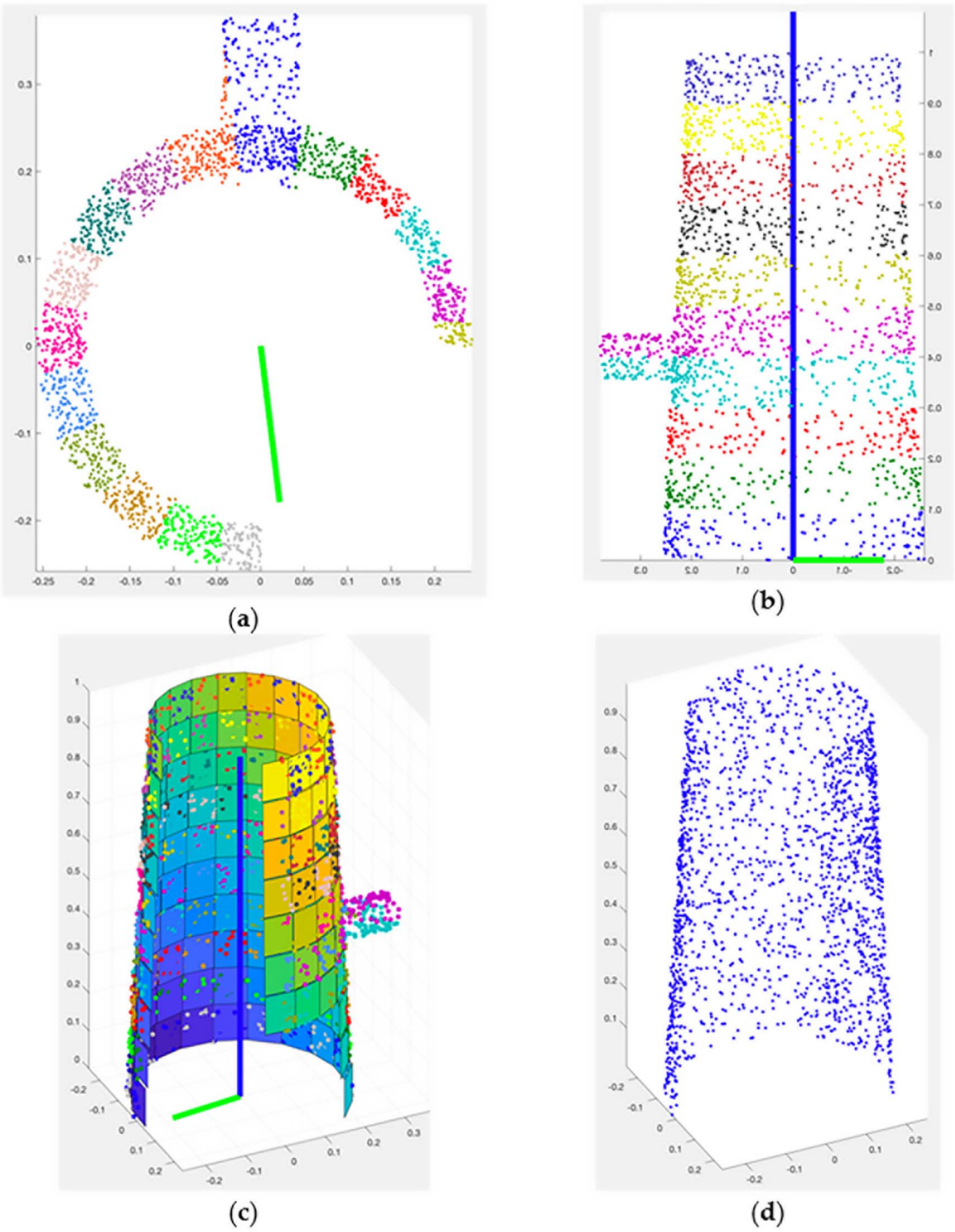

Figure 6 Determination of cylindrical surface coverage. Potential stem section is partitioned into (a) equal-angle sectors based on a line (green) orthogonal to the cylinder axis (blue) and (b) equal-height layers based on the axis. (c) The final partition is the intersection of the sectors and layers and the surface coverage is the relative number of non-empty intersections. (d) Filtering based on the partition where only the points closest to the axis from each subset are kept. Different colours denote different subsets.

algorithm to each of the 18 point clouds produced with the photogrammetric method. In addition to the total number (trees found in at least one iteration), the table also shows the number of trees found in all 10 iterations and those found in at least 9 iterations. All 45 trees were found only in the point clouds generated with Image scale ¼ or ½. At the same time, with Image scale ½, it was possible to find all trees with the Point density set to high and optimal. When our algorithm was used

Table 2 Number of trees found in different point clouds.

Point cloud index	Number of found trees		
	Total	In all the 10 iterations	In at least 9 iterations
1	44	39	40
2	44	43	44
3	32	23	23
4	37	35	36
5	45	43	45
6	43	42	42
7	42	39	40
8	45	43	44
9	44	43	43
10	45	45	45
11	45	45	45
12	45	43	45
13	45	41	43
14	45	45	45
15	45	44	45
16	45	45	45
17	45	44	44
18	36	34	34

on the point cloud generated with the Image scale $^1/_2$ and low density (point cloud 18), only 36 trees were found.

The most problematic point cloud is n. 3, which was produced with the lowest density parameters (Image scale: 1/8; Point density: low; Minimum number of matches: 3). However, despite these problems, the algorithm was able to reconstruct 32 trees from the different iterations. All the trees were found in all the 10 iterations in point clouds 10, 11, 14 and 16. Interestingly, all these point clouds were produced with an Image scale of $^1/_2$, except for n. 10 (Image scale: 1/4; Point density: low; Minimum number of matches: 3).

We also investigated in how many point clouds each tree in the plot was reconstructed by applying the algorithm. A total of 12 of the 45 trees were reconstructed in all 10 iterations of the 18 point clouds and another 20 in at least 9 iterations of them.

Mapping these data for each tree (Figure 7) shows that the most problematic trees were those photographed only in the first two stretches of the forward survey path and in all the photos taken during the return survey. These photos were taken under non-optimal light conditions of backlighting due to the position of the sun and most had significant lighting problems.

Cylinder-based d.b.h. estimates from different point clouds

The RMSE and d.b.h. bias estimated by the cylinder-fitting approach compared with the field data of those point clouds with all the 45 trees reconstructed are summarized in Table 3. Mean standard deviations and absolute errors were also calculated for the 18 point clouds (Table 4).

D.b.h. RMSE values ranged from a minimum of 1.6 cm (5.58 per cent) to a maximum of 4.6 cm (16.09 per cent). The best result in terms of RMSE was achieved by point cloud 10 (Image scale: 1/4; Point density: low; Minimum number of matches: 3). This point cloud also had the lowest bias value. A strong correlation was also found between the d.b.h. measured in the field and the d.b.h. derived with the cylinder-fitting approach based on this point cloud ($R^2 = 0.95$) (Figure 8). This point cloud also had the lowest mean absolute error (0.58 cm), low uncertainty and high precision as indicated by the low mean standard deviation in the estimation of the d.b.h. (0.23 cm) (Table 4). However, the best result in terms of mean standard deviation was shown by point cloud 14 (Image scale: 1/2; Point density: optimal; Minimum number of matches: 3—the default settings of the software). The d.b.h. RMSE value of this point cloud was also good (RMSE = 2.14 cm; RMSE% = 7.72). Negative bias values indicate that the model tends to slightly underestimate d.b.h.

Figure 9 compares the average absolute error and standard deviations of d.b.h. estimates, both from the 10 modelling iterations, for each tree and for each point cloud. Point clouds 1 and 2 have a high level of error and standard deviation, showing poor results in terms of accuracy and uncertainty. The best accuracy and uncertainty results were obtained from point cloud 10, with a maximum average error value of 2.9 cm and standard deviation of <0.5 cm for all but three of the trees. Figure 9a shows the standard deviation of the d.b.h. estimates obtained during the 10 iterations and for each tree in the different point clouds. The comparison of these values between the number of trees and number of point clouds highlights how well the algorithm worked in most cases. In point clouds 1 and 2, the standard deviation is large for almost every tree. In the other point clouds, except for point cloud 18, trees 37–45 usually have large standard deviations. Tree 27 had some problems in most of the point clouds, with standard deviation values of ~3–4 cm. Of note is the peak in the standard deviation values at tree 10 for point clouds 11 and 12. As shown in Figure 9b, absolute error values are bigger than standard deviations, in particular in the first four point clouds. In addition, in most cases, the most problematic trees in terms of accuracy are trees 1–10 and trees 35–45, which were those captured in a smaller number of images because they were located at the beginning of the two photographic paths.

Volume estimates by sections from different point clouds

Volumes by sections, estimated using diameters measured at different heights of up to 6 m with a Wheeler pentaprism, were compared with those obtained using the Section Model. These data were also compared to section volumes given by the Extraction Model. Depending on the quality of the point clouds, it was not possible to use all 15 reference trees to calculate section volumes in all the point clouds. Table 5 summarizes the RMSE of the section volumes and the bias for the 9 point clouds in which the model managed to compute section volumes of up to 6 m for all the 15 reference trees. The minimum RMSE value (22.67 per cent) was obtained from point cloud 10 (Image scale: 1/4; Point density: low; Minimum number of matches: 3). Estimated section volumes obtained from point cloud 10 correlated strongly with those calculated by field measurements ($R^2 = 0.872$, Figure 10). Extraction Model RMSE and bias values were considerably smaller than those obtained with the Section Model (but see standard deviation results below).

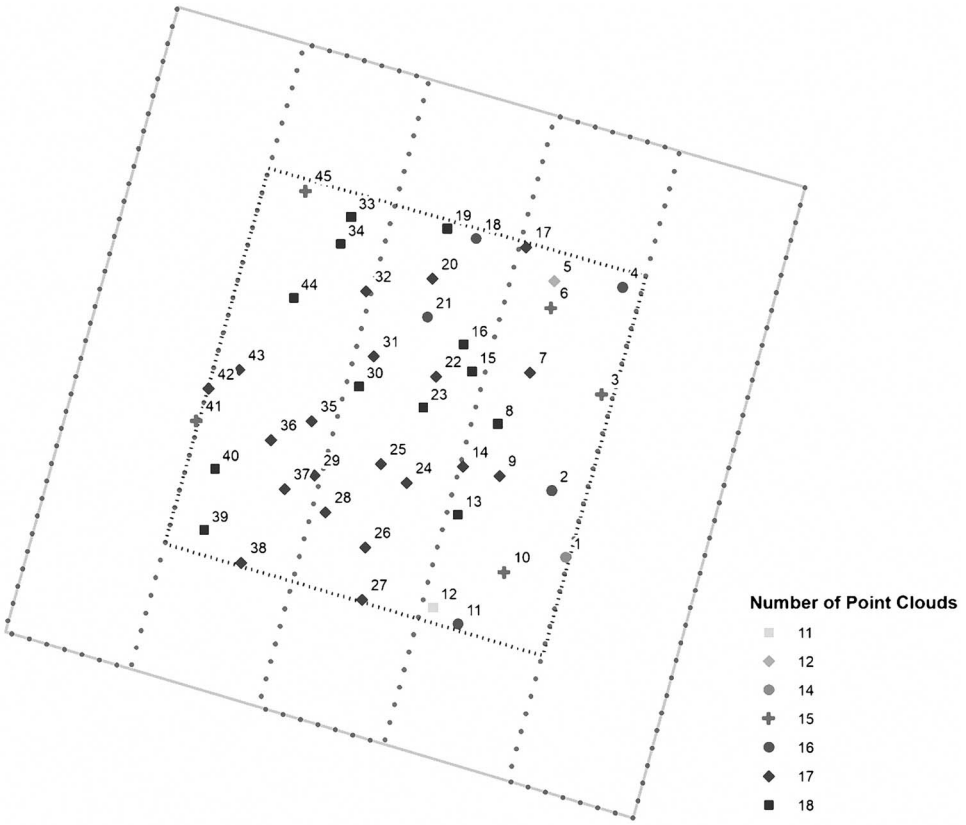

Figure 7 Map of trees showing in how many point clouds each tree was found in at least 9 out of 10 iterations. Dotted line indicates the route of the forward survey path.

Table 3 Extraction Model d.b.h. results—RMSE and bias.

Point cloud index	Number of reconstructed trees	RMSE d.b.h.		Bias d.b.h.	
		(cm)	%	(cm)	%
1	44	–	–	–	–
2	44	–	–	–	–
3	32	–	–	–	–
4	37	–	–	–	–
5	45	3.0991	10.71	−2.04	−7.07
6	43	–	–	–	–
7	42	–	–	–	–
8	45	2.3479	8.12	−1.05	−3.63
9	44	–	–	–	–
10	45	1.6142	5.58	−0.58	−1.99
11	45	2.2669	7.84	−1.30	−4.50
12	45	2.9589	10.23	−1.60	−5.52
13	45	4.6561	16.09	−2.03	−7.01
14	45	2.1468	7.42	−1.10	−3.82
15	45	2.6816	9.27	−1.61	−5.56
16	45	1.7768	6.14	−0.71	−2.45
17	45	2.3661	8.18	−0.97	−3.36
18	36	–	–	–	–

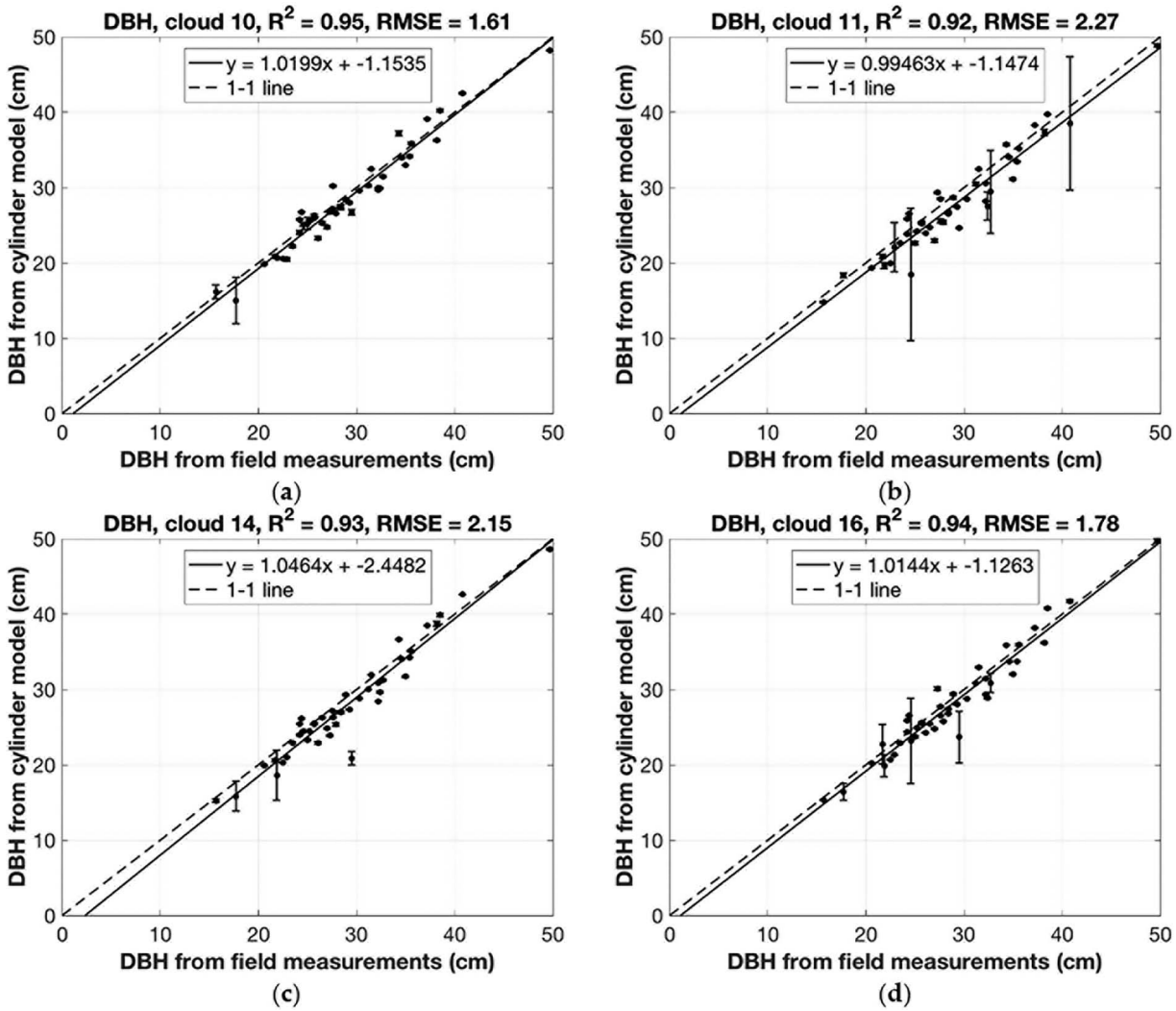

Figure 8 D.b.h. estimated by the cylinder-fitting approach compared with field measured d.b.h. Results of the point clouds that detected all trees in all 10 iterations are illustrated. The depicted values are averages calculated from the 10 iterations and the error bars/vertical bars show ±SD of the iterations. (a) point cloud n. 10, (b) point cloud n. 11, (c) point cloud n. 14 and (d) Point cloud n. 16. Results of all the remaining point clouds are available in Supplementary Figure 8.

Similar to the d.b.h. estimates, we analysed the average absolute error and standard deviations of volumes computed from the 10 iterations for each tree and each point cloud in order to estimate the uncertainty and the accuracy of the Section Model. Volume estimates by the Section Model on point cloud 1 show the highest average error values while those on point cloud 10 the lowest (Table 6). Mean absolute error values for each tree also showed that volume estimates for tree 10 (dark grey column in the table) were the least accurate, while those for tree 17 (light grey column in the table) were the most accurate, with mean absolute error values higher than 0.04 m^3 only from point clouds 1 and 2. Table 7 summarizes the standard deviation values of the section volumes from each point cloud obtained using the Section Model for all the 15 trees measured in field. These values were highest for tree 42 (dark grey column) and lowest for tree 25 (light grey column) in most point clouds. Therefore, the volume estimates of tree 42 were the most uncertain, while those of tree 25 were the most precise. The most problematic point clouds were 1 and 13, with values up to 0.05593 m^3. These point clouds produced results with the highest uncertainty, while estimates from point cloud 10 were the most precise in the Section modelling.

A comparison of the Section Model and Extraction Model results highlights that the Extraction Model gave more accurate volume estimates, but that the higher standard deviations indicate more uncertainty in these estimates (Figure 11).

Correlation coefficients

An initial analysis of the results seems to indicate that the densification parameters have a significant influence on the results. To estimate the influence more quantitatively, we calculated the

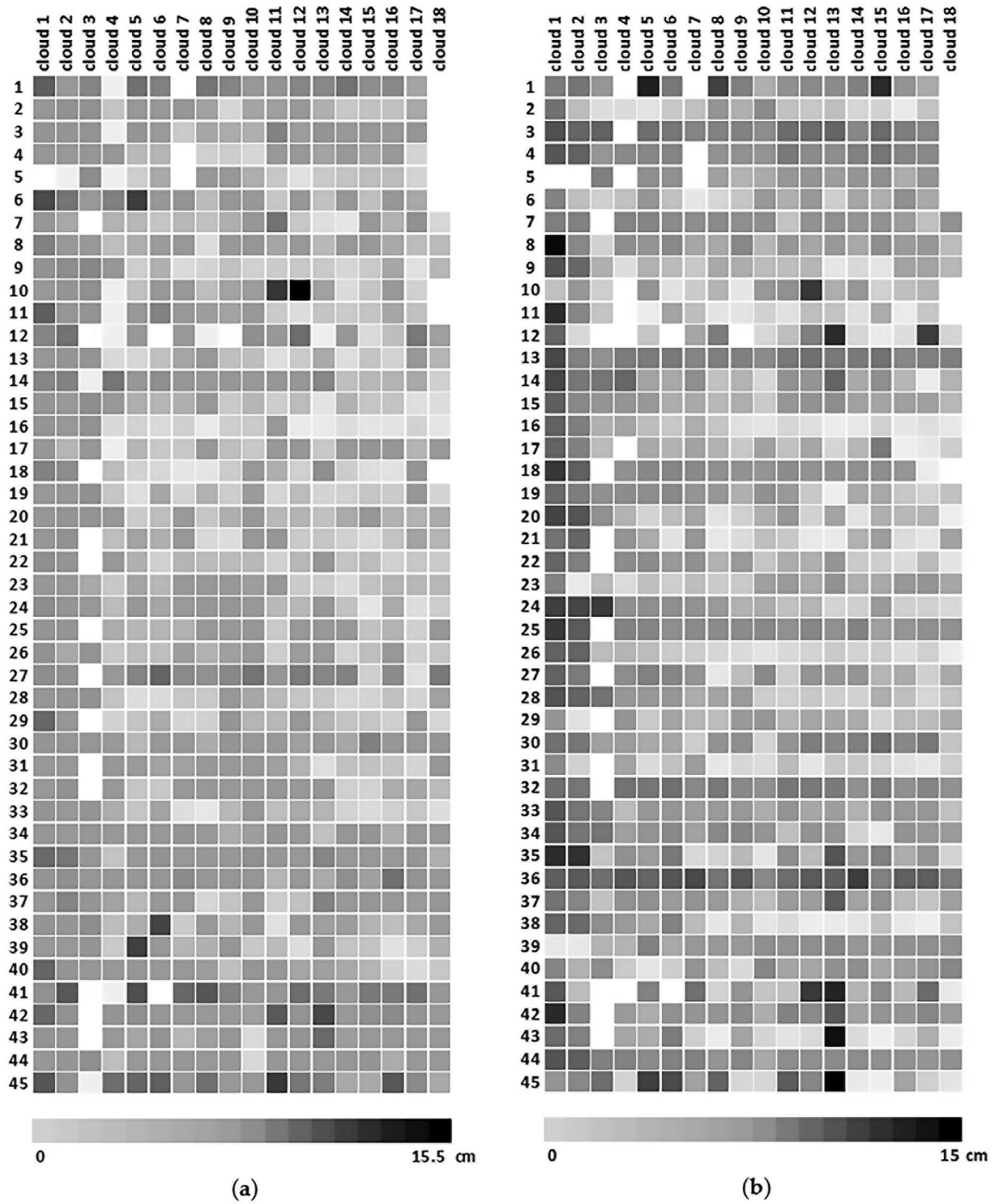

Figure 9 Standard deviation and mean absolute error of d.b.h. for each tree in the 18 point clouds obtained during the 10 iterations. (a) Standard deviation and (b) absolute error. White pixels indicate that the tree was not detected in the corresponding point cloud.

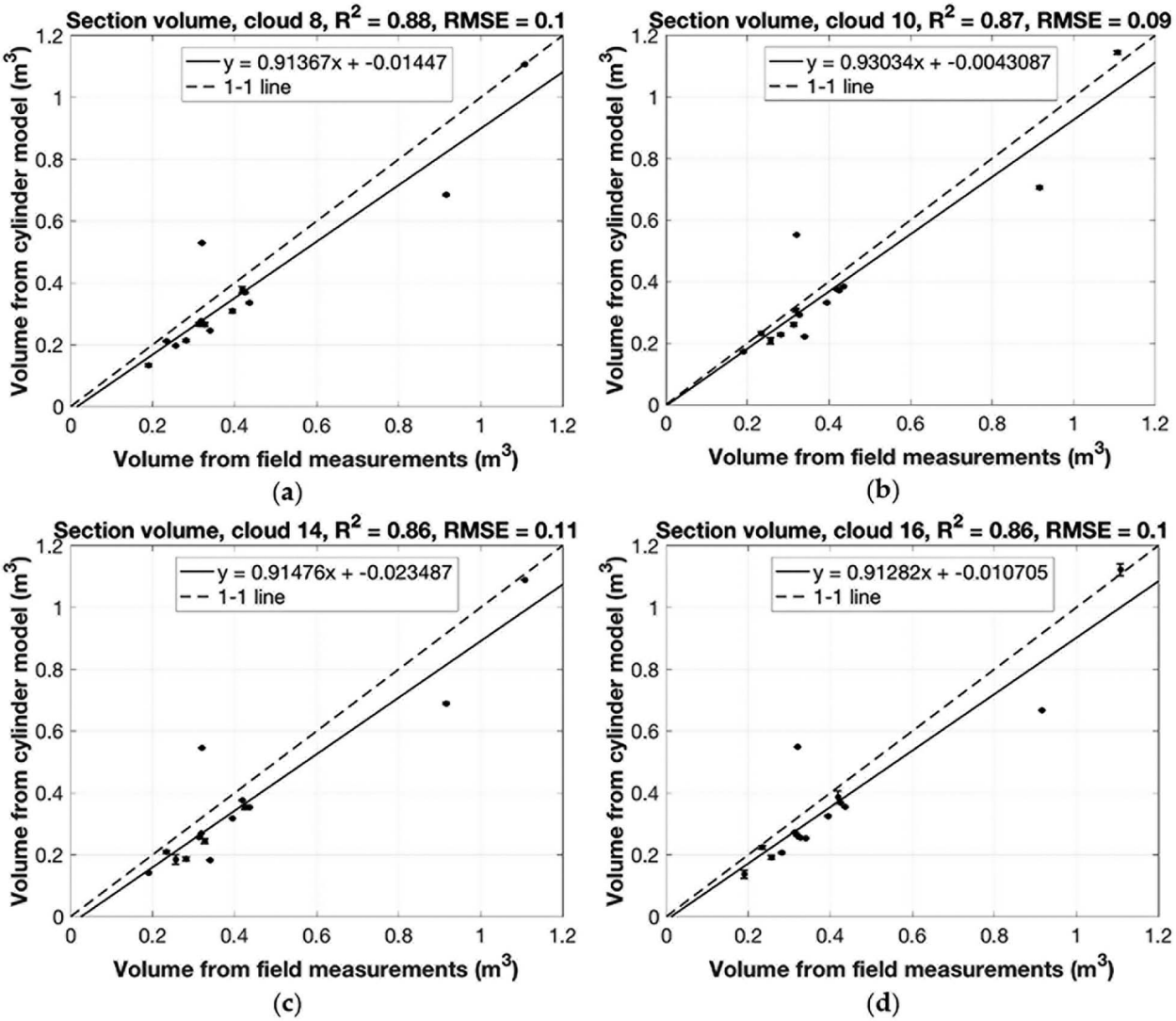

Figure 10 Volumes from Section Model compared with field measured volume by sections. The values are averages calculated from the 10 iterations and the error bars/vertical bars show ±SD of the iterations. (a) Point cloud n. 8, (b) point cloud n. 10, (c) point cloud n. 14 and (d) Point cloud n. 16. Results of all the remaining point clouds are available in Supplementary Figure 10.

correlation coefficients of these parameters with the following variables: number of reconstructed trees; RMSE and standard deviation of d.b.h.; volume RMSE and standard deviation from the Section Model (Table 8). The number of reconstructed trees showed a low correlation with the Image scale and a low–medium correlation with Point density and Minimum number of matches. On the other hand, the correlation of the RMSE of d.b.h. correlated poorly with Image scale, but correlated highly with Point density and Minimum number of matches. Thus, errors in d.b.h. estimates increase with increasing Point density and Minimum number of matches. The correlation of RMSE of volume with densification parameters gave very different results: a medium negative correlation with Image scale and Minimum number of matches (RMSE increases with decreasing Image scale and Minimum number of matches) and a medium positive correlation with Point density. The standard deviation of d.b.h. and volume showed similar correlations to the corresponding RMSE correlations. The standard deviation of d.b.h. shows a high correlation with point density and a medium correlation with Minimum number of matches, while the standard deviation of volume shows a negative correlation with Image scale and Minimum number of matches.

Discussion

The use of photogrammetric methods to estimate biometric parameters in the forest is still a developing field. Forests often have complex light conditions, high tree densities and occlusions by branches and shrubs can occur. This makes photogrammetric measurements challenging, and investigations are needed to for example identify optimal acquisition paths and processing

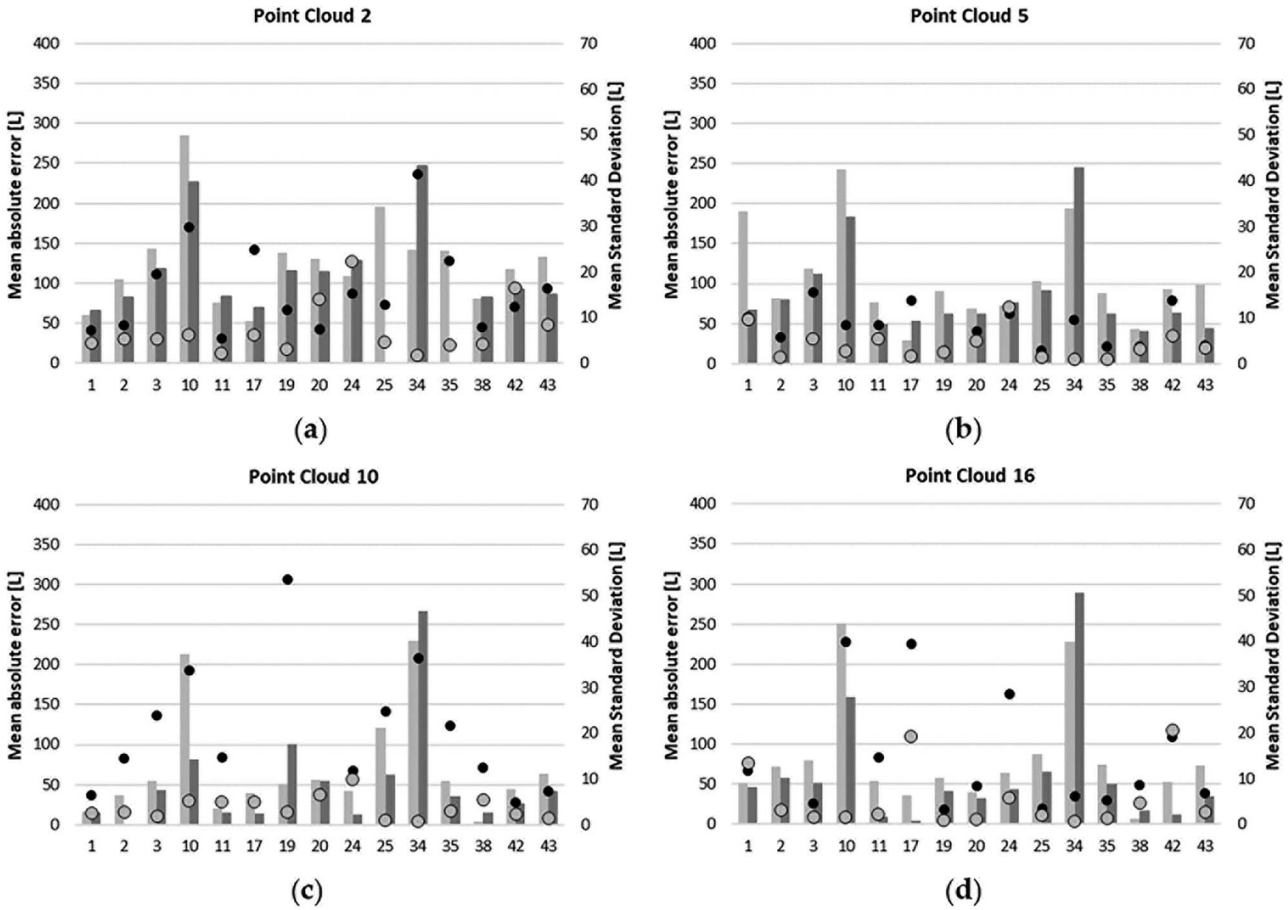

Figure 11 Mean absolute error [L] (left y-axis) and mean standard deviation [L] (right y-axis) of section volume estimates from modelling each point cloud. Bars indicate mean absolute errors, while dots indicate standard deviations (light grey: Extraction Model; dark grey: Section Model). (a) Point cloud n. 2, (b) point cloud n. 5, (c) point cloud n. 10 and (d) Point cloud n. 16. Results of all the remaining point clouds are available in Supplementary Figure 11.

Table 4 Extraction Model d.b.h. results—mean absolute error and standard deviation.

Point cloud index	Mean absolute error (cm)	Mean standard deviation (cm)
5	2.04	0.8233
8	1.05	0.3730
10	0.58	0.2342
11	1.30	0.7460
12	1.60	0.7693
13	2.03	0.6282
14	1.10	0.2209
15	1.61	0.2419
16	0.71	0.4186
17	0.97	0.2876

parameters for deriving dendrometric inventory data from these data.

In this study, we examined several of these parameters using photogrammetric surveys based on a smartphone camera. The use of terrestrial image-based point clouds from a smartphone camera—a non-specialized instrument that almost everyone owns—is a new and straightforward way to investigate the structure and features of forest plots. To our knowledge, in the published literature so far only professional cameras were used to produce point clouds of forest stands. This paper has explored the feasibility of using this low-cost photogrammetric method for the collection of forest inventory data and has compared the quality of the terrestrial photogrammetric point clouds obtained with different densification parameters of the point clouds.

In this section, we present a comparison of our results with those obtained in previous studies, although the comparison must take into account the presence of random errors in the estimation of the parameters in the field in the various studies, as well as general differences in the species composition and the complexity of the investigated forest stands.

Liang *et al.* (2015) developed several photogrammetric methods to estimate d.b.h. in a 30 × 30 m field plot with 25 trees (mean d.b.h. = 31.86 cm), i.e. with a tree density of ∼50 per cent of our plot. They obtained d.b.h. estimates with an RMSE ranging from 2.98 cm (8.03 per cent) to 6.79 cm (18.87 per

Table 5 Volume estimates by sections ($h = 6$ m).

Point cloud index	Section Model				Extraction Model			
	RMSE section volume (m^3)	%	Bias section volume (m^3)	%	RMSE section volume (m^3)	%	Bias section volume (m^3)	%
1	0.185569	44.39	−0.1631	−38.93	0.170347	40.65	−0.1408	−33.61
2	0.136495	33.30	−0.1095	−26.13	0.130566	31.16	−0.0951	−22.71
5	0.112862	26.93	−0.0736	−17.59	0.104982	25.05	−0.0494	−11.80
8	0.099392	23.72	−0.0506	−12.09	0.087235	20.82	−0.0312	−7.46
10	0.094983	22.67	−0.0335	−7.99	0.085458	20.39	0.0001	0.02
11	0.12036	27.93	−0.0655	−15.65	0.098021	23.39	−0.0371	−8.85
12	0.131031	27.34	−0.0646	−15.43	0.098181	23.43	−0.0478	−11.41
14	0.108853	25.98	−0.0592	−14.13	0.097816	23.34	−0.0383	−9.14
16	0.103580	24.72	−0.0472	−11.27	0.095426	22.77	−0.0270	−6.46

Table 6 Section volume mean absolute error [L].

		Tree index														
		1	2	3	10	11	17	19	20	24	25	34	35	38	42	43
Point	1	190.4	171.4	436.5	348.1	151.2	89.3	172.9	313.6	256.7	238.6	93.6	226.4	127.3	198.9	203.4
cloud	2	59.5	105.2	143.6	285.5	75.4	52.2	138.6	130.6	108.5	195.4	142.3	140.5	80.0	117.1	133.2
index	3	36.2	54.5	85.7	196.2	59.8	11.6	76.1	94.7	256.8		198.9	96.3	234.3	117.1	133.2
	4		84.5					87.2	86.3	256.8	157.5	177.4	105.0	59.5	98.8	129.6
	5	190.5	81.7	118.0	242.7	76.7	28.8	89.9	68.4	72.5	102.9	194.4	88.2	42.9	92.6	98.6
	6	71.9	94.6	161.0	289.0	100.4	18.7	82.2	64.7	256.8	105.2	194.4	76.0		92.9	80.4
	7		68.4	85.2	916.5	58.3	2.3	71.1	62.6	67.8	129.5	204.7	78.7	35.4	77.2	92.5
	8	51.7	59.5	99.1	229.0	41.7	0.1	55.3	48.9	61.4	95.1	210.1	64.9	20.4	56.0	85.8
	9	40.0	40.0	42.6	241.5		4.4	54.5	32.4	62.6	81.5	209.8	53.1	8.0	60.2	75.0
	10	16.7	37.1	54.4	213.6	20.4	39.1	51.0	55.8	41.5	121.2	230.4	55.2	3.0	44.9	63.3
	11	60.8	69.3	101.0	282.3	71.7	37.1	77.8	65.1	72.8	113.9	213.5	86.4	27.9	41.1	85.1
	12	51.9	45.5	107.5	262.1	318.7	2.1	63.0	59.4	256.8	92.4	221.3	83.5	46.4	419.2	103.7
	13	25.3	73.2	5.3	279.7		26.5		93.1	256.8		215.7	93.5	41.5	143.3	395.1
	14	49.9	92.1	82.9	230.1	51.0	20.2	67.2	59.1	68.8	156.7	223.8	103.0	27.8	43.2	78.0
	15	59.6	54.3	124.5	279.3		29.0	68.6	56.7	48.7	92.2	200.6	81.7	12.1	81.1	77.3
	16	51.2	71.7	80.0	250.3	54.0	36.3	57.4	40.3	63.7	87.4	228.3	75.1	7.0	52.9	72.9
	17	52.2	32.7	110.5	229.8		23.9	57.9	53.7	65.6	85.9	228.5	81.2	234.3	22.7	81.8
	18						16.1	32.3	66.7	67.1	138.7	230.9	58.2	4.9	35.3	64.4

cent). More recently, Piermattei *et al.* (2019) estimated d.b.h. and stem curves (up to 2.8 m above the ground), using a cylinder-fitting method, in four forest plots with a tree density ranging from 390 to 875 stems ha^{-1}. They estimated d.b.h. with an RMSE between 1.21 and 5.07 cm. To our knowledge, until now these are the only studies that used cylinder modelling to estimate stem diameters.

Forsman *et al.* (2016) developed a method to estimate d.b.h. with image-based techniques in six circular field plots (20-m radius). They obtained the best RMSE (2.6 cm) in the plot with a tree density of 270 trees ha^{-1} (mean d.b.h. = 21.0 cm) and the worst (13.8 cm) in the plot with ∼300 trees ha^{-1} (mean d.b.h. = 22.8 cm). Mikita *et al.* (2016) estimated d.b.h. and stem volume of 118 trees (mean d.b.h. = 38.16 cm) in a 0.8 ha forest stand, with tree density of 30 per cent of our plot. D.b.h. estimates used a circle-fitting method and stem volumes were calculated by an allometric equation. They reported a d.b.h. RMSE of 0.911 cm (2.39 per cent) and a volume RMSE of 0.082 m^3.

The forest plots studied in these published articles are broadly comparable with that of the present study. It is hence interesting that the RMSE values found in this study (d.b.h. RMSE = 1.61 cm and stem volume RMSE = 0.094 m^3) are better than those presented in all the previous studies, except for Mikita *et al.* (2016). The latter is the only study that estimated stem volumes, in addition to the d.b.h., but the volume estimates were based on allometric relationships. The better performances observed in the study of Mikita *et al.* (2016) could be due to the lower density of trees in their forest plot compared to that of our study and due to the availability of well-suited allometries.

Table 7 Section volume standard deviation [L].

		Tree index														
		1	2	3	10	11	17	19	20	24	25	34	35	38	42	43
Point	1	18.46	7.77	13.78	7.04	17.11	12.99	3.22	5.86	4.78	3.36	3.44	26.97	14.20	11.54	12.87
cloud	2	4.46	5.21	5.30	6.24	2.02	6.13	2.98	14.01	22.16	4.62	1.69	3.90	4.25	16.55	8.48
Index	3	5.45	16.64	5.55	23.92	9.80	13.18	11.22	8.57			3.33	0.39			
	4		0.54					0.82	1.09	4.96	0.50	1.48	2.79	9.27	5.12	1.96
	5	9.71	1.30	5.39	2.75	5.44	1.74	2.50	5.06	12.36	1.50	1.05	1.03	3.13	6.17	3.33
	6	5.94	7.59	22.21	8.29	29.94	0.89	2.73	4.55	7.89	0.53	1.09	6.29		17.47	4.75
	7		1.18	5.48	3.56	2.06	1.00	0.97	0.85	1.58	0.82	1.13	2.57	1.30	1.81	1.11
	8	5.09	5.94	2.45	2.21	1.24	0.89	2.59	4.99	1.27	0.62	1.09	3.70	1.35	9.69	5.75
	9	4.54	18.90	43.36	3.54		1.23	0.93	2.46	6.78	3.38	0.63	14.92	4.01	41.53	1.62
	10	2.63	2.76	1.86	5.19	5.00	4.90	2.71	6.64	9.96	1.00	0.65	2.90	5.46	2.32	1.46
	11	2.69	1.14	7.55	8.27	2.27	17.02	2.38	100	17.88	0.96	1.08	6.91	5.36	56.42	12.75
	12	3.82	5.12	5.84	9.14		1.01	1.92	1.19	10.33	1.16	0.92	3.58	7.99	20.23	4.47
	13	37.48	12.97	55.92	25.87		1.20		16.91	29.71		1.28	5.96	24.56	21.84	
	14	1.80	8.12	1.46	3.14	0.79	1.19	7.09	1.03	14.95	0.90	0.67	5.53	3.62	0.98	1.24
	15	6.14	3.45	6.31	0.92		1.70	1.26	0.85	0.72	0.60	1.31	1.11	1.98	1.16	1.15
	16	13.46	3.03	1.52	1.42	2.28	19.15	0.77	1.02	5.82	1.89	0.57	1.25	4.62	20.56	2.73
	17	1.73	8.08	28.77	11.27		1.13	3.66	1.63	4.74	1.09	0.50	1.15	9.47	18.23	1.02
	18						1.38	0.52	15.12	6.98	2.24	0.85	1.72	2.64	0.96	1.73

Table 8 Correlation coefficient with densification parameters.

	Image scale	Point density	Minimum no. of matches
No. of reconstructed trees	0.282191166	0.423233178	0.442913404
RMSE d.b.h.	0.186784026	0.700465172	0.803823716
RMSE volume	−0.524342322	0.483270612	−0.352826843
SD d.b.h.	0.071999959	0.898297643	0.455042236
SD volume	−0.210754747	0.539382044	−0.165215077

Our experiment highlighted strengths and weaknesses of the applied image acquisition grid. It is evident that the photogrammetric process has given better results for trees located towards the centre of the plot. This is probably because these trees are captured by a larger number of images in both the forward and the return survey paths. It is therefore important to maximize the number of images in which each element of the scene is present, in order to obtain good results with the photogrammetric reconstruction of the trees.

Light conditions are another factor to take into account when setting the image acquisition grid, because they greatly affect the quality of the point clouds and consequently the performance of the model. It is advisable to avoid lighting problems during the photographic survey. For example, images captured when the sun is higher or during the early afternoon (when there is a softer light in the forest) prevent the acquisition of images against the light. Similarly, an overcast sky also prevents lighting problems (Liang *et al.*, 2015; Forsman *et al.*, 2016; Piermattei *et al.*, 2019).

Recent studies demonstrated that the accuracy of photogrammetric point clouds varies with the resolution of the image sensor, the camera configuration and the equipment used to support the camera (Piermattei *et al.*, 2019). In this study, we also investigated the influence of densification parameters on the 3D reconstruction and, hence, on d.b.h. and volume estimates. The results showed that Image scale is the parameter that most influences the model's performance in finding and extracting trees from the point clouds. All the trees were found in all the 10 modelling iterations in point clouds produced with an Image scale of $^1/_2$. The only point cloud produced with an Image scale different from $^1/_2$ that allowed to find all the 45 trees was the number 10 (Image scale: 1/4; Point density: low; Minimum number of matches: 3). Details in the images increase as the image scale increases, which improves the production of the point cloud during the photogrammetric process.

Therefore, using a higher Image scale value (increasing the image size during the photogrammetric process for the production of the point cloud and therefore the possibility to obtain more details) leads to a better reconstruction of the 3D structure of the trees, reducing the presence of noise caused by incorrectly identified points. Nevertheless, it is important to make the right combination of this parameter with the other parameters. The results show that the best performance for extracting d.b.h. and volume estimates for the individual tree was obtained with point cloud 10 (Image scale: 1/4; Point density: low; Minimum number of matches: 3). This indicates that a low density of the point cloud can positively influence the volume estimates, probably due to reduced noise. It is therefore possible to state that the presence of incorrectly positioned points (noise) and an excessively high Point density lead to incorrect fitting of cylinders to the stems and consequently cause errors in the estimates of biometric forest inventory parameters. Point cloud 10 also gave the best results

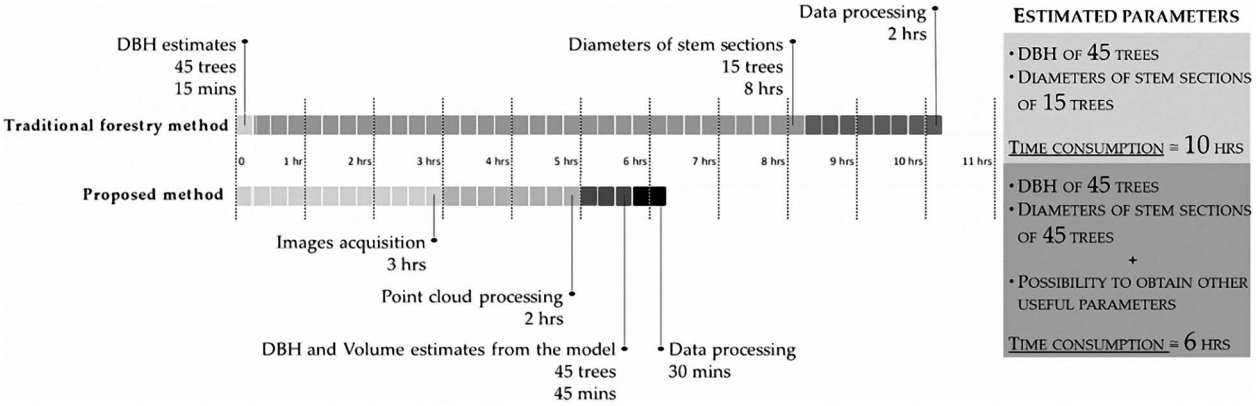

Figure 12 Working timeline comparison between the two methods.

in terms of accuracy and uncertainty with very low values of standard deviation and average error from the 10 iterations of the Section Model. Maintaining the same Point density and Minimum number of matches and improving the Image scale from 1/8 to 1/4 can lead to a substantial change in results, improving the worst result (point cloud 3 with Point density low, Minimum number of matches 3 and Image scale 1/8) into one of the best (point cloud 10).

Besides assessing the influence of the densification parameters of the SfM algorithm, we also examined two different approaches to estimate the stem volume: the Extraction Model and the Section Model. The former models the stem with cylinders of variable height, while the latter uses 1 m tall stem sections (to compare model estimates with those obtained from data collected in the field). We found that volumes estimated by the Extraction Model generally gave lower RMSE values than the Section Model, and lower values of absolute error, but high values of standard deviation. This is probably because on the one hand the cylinders in the Extraction Model are generally shorter and can thus more accurately fit the local diameter. On the other hand, standard deviation is larger with the Extraction Model because the lengths and sections of the fitted cylinders can change from one iteration to the other, in contrast to the Section Model, where the sections are always the same. Thus, it could be possible to estimate volumes using only the Extraction Model, given its good correspondence with the total stem volume up to a certain height, as estimated with the traditional dendrometric method.

Concerning the efficiency of the presented approach, we found that the traditional method of estimating the examined forest inventory metrics, particularly the diameters of stem sections at multiple heights, is more time-consuming than the proposed method. The suggested approach takes approximately half the time that the traditional methods require (estimated time based on experience) (Figure 12). Furthermore, it is possible to obtain other dendrometric parameters useful for forest management and planning purposes (in addition to d.b.h. and volume) including lower crown height, or crown depth estimated by combining images from the ground with aerial images, simply by implementing the estimation algorithm. Furthermore, it could be possible to use the photographic surveys as presented in this study: (1) to estimate all the parameters needed to produce volume tables rapidly and without felling trees; (2) to carry out thinning simulations, estimating the possible withdrawable assortments of wood and the residual volume; repeated photographic surveys would additionally allow for, (3) carrying out multi-temporal surveys in order to estimate stand growth over time and to monitor the evolution of forest stands.

In summary, our results show that photogrammetric point clouds can be useful for the reconstruction of 3D tree models to derive diameter and volumes estimates. Although d.b.h. and volumes were underestimated in comparison with those obtained using data collected in the field, both d.b.h. and volume up to a height of 6 m were estimated with good accuracies. Since it is not possible to assess the error in the estimates produced by the field measurements conducted here (attempting to measure irregular shapes, i.e. defined by the presence of ribs or irregularity of the bark) and the photogrammetric 3D model (dependent on many factors, including the image calibration process), it is not possible to define which method is more reliable. This would require to fell some of the trees and to measure the targeted parameters, which was out of the scope of this study. Nevertheless, it is encouraging to see that the estimates produced by the photogrammetric approach agreed very well with the measurements of the traditional approach and that the data collection was less time-intensive. Even though certain hardware and software requirements have to be fulfilled for subsequent data processing, a further optimization of the process may also result in a significant cost-saving.

Conclusions

We presented a rapid and automatic image-based, photogrammetric method for estimating diameters from multiple heights of a stem as well as the stem's volume. These parameters are difficult to assess in the field, and the suggested approach is a real alternative to other non-destructive measurements of stem volume and diameters at multiple heights and allows the structure of forest stands to be studied in a more objective way.

The possibility to obtain a 3D reconstruction of forest stands makes it possible to acquire the nearly complete structure of

the studied stand. This information could be used to estimate other forest inventory metrics useful for forest management and planning purposes, which may be calculated using the point cloud.

We tested the influence of the densification parameters of the photogrammetric process on the d.b.h. and volume estimates of our method, finding that the most important parameter is Image scale. Furthermore, our results suggest that it is important to find an optimal balance between Point density and Image scale.

We tested our method in a stand with relatively simple structure, but we are confident that it will work well even in forests with more understory, if the understory does not cover most of the stem. Further studies are in progress to test the performance of the method under such conditions.

The future challenge will be to estimate total tree volume by improving the photogrammetric survey to capture also the upper part of the stem by changing the settings of the survey path and modifying the tree modelling approach. This could enable the extraction of the total tree structure to estimate total volume and other useful dendrometric parameters for forest management, such as lower crown-base height, or also crown depth when the images taken on the ground are combined with images captured by a drone. The performance of the presented approach may further improve with the technological evolution of smartphone cameras.

Supplementary data

Supplementary data are available at *Forestry* online.

Funding

Studio sperimentale della pianificazione assestamentale avanzata relativa ai complessi forestali di proprietà della Regione Puglia gestiti dall'A.R.I.F.'; Agenzia Regionale per le attività irrigue e forestali A.R.I.F. Puglia (Italy) (agreement between A.R.I.F. Puglia (Italy) and the Department of Agricultural and Environmental Sciences of the University of Bari Aldo Moro (Italy)). 3DForMod project, ERA-NET FACCE ERA-GAS (ANR-17-EGAS-0002-01); European Union's Horizon 2020 research and innovation program (grant agreement No. 696356 to FACCE ERA-GAS).

Conflict of interest

None declared.

Acknowledgements

This study was funded by the agreement between the Agenzia regionale per le attività irrigue e forestali, A.R.I.F. Puglia (Italy) and the Department of Agricultural and Environmental Sciences of the University of Bari Aldo Moro (Italy). Studio sperimentale della pianificazione assestamentale avanzata relativa ai complessi forestali di proprietà della Regione Puglia gestiti dall'A.R.I.F. . We would like to thank workers of the regional agency A.R.I.F. Puglia for helping with the survey activities. The authors are grateful to the associate editor (Dr F. Fassnacht) and two anonymous reviewers for suggestions that considerably improved the manuscript.

References

1 Åkerblom, M., Raumonen, P., Kaasalainen, M. and Casella, E., 2015 Analysis of geometric primitives in quantitative structure models of tree stems. *Remote Sens.* **7**, 4581–4603. doi: 10.3390/rs70404581.

2 Bakker, M. and Lane, S.N., 2017 Archival photogrammetric analysis of river-floodplain systems using structure from motion (SfM) methods: Archival photogrammetric analysis of river systems using SfM methods. *Earth Surf. Proc. Land.* **42**, 1274–1286. doi: 10.1002/esp.4085.

3 Bay, H., Ess, A., Tuytelaars, T. and Van Gool, L., 2008 Speeded-up robust features (SURF). *Comput. Vis. Image Und.* **110**, 346–359. doi: 10.1016/j.cviu.2007.09.014.

4 Brink, C. and Gadow, K.V., 1986 On the use of growth and decay functions for modeling stem profiles. *EDV in Medizin und Biologie* **17**, 20–27.

5 Calders K., Newnham G., Burt A., Murphy S., Raumonen P., Herold M., *et al.* 2015. Nondestructive estimates of above-ground biomass using terrestrial laser scanning. *Methods Ecol. Evol.* **6**(2), 198–208. doi:10.1111/2041-210X.12301

6 Cavegn, S., Haala, N., Nebiker, S., Rothermel, M. and Tutzauer, P., 2014 Benchmarking high density image matching for oblique airborne imagery. *ISPRS—Int. Arch. Photogramm. Remote Sens. Spat. Inf. Sci* **XL–3**, 45–52. doi: 10.5194/isprsarchives-XL-3-45-2014.

7 Dassot, M., Colin, A., Santenoise, P., Fournier, M. and Constant, T., 2012 Terrestrial laser scanning for measuring the solid wood volume, including branches, of adult standing trees in the forest environment. Computers and electronics in agriculture. *Comput. Electron. Agr* **89**, 86–93. doi: 10.1016/j.compag.2012.08.005.

8 Dhôte, J.F., Hatsch, E. and Rittié, F., 2000 Forme de la tige, tarifs de cubage et ventilation de la production en volume chez le Chêne sessile. *Ann. For. Sci.* **57**, 121–142.

9 Forsman, M., Börlin, N. and Holmgren, J., 2016 Estimation of tree stem attributes using terrestrial photogrammetry with a camera rig. *Forests.* **7**, 61. doi: 10.3390/f7030061.

10 Gaffrey D., Sloboda B., Matsumura N., 1998. Representation of tree stem taper curves and their dynamic, using a linear model and the centroaffine transformation. *J. For. Res.*, **3**(2). 67–74.

11 Giannetti, F., Puletti, N., Quatrini, V., Travaglini, D., Bottalico, F., Corona, P., *et al.* 2018. Integrating terrestrial and airborne laser scanning for the assessment of single-tree attributes in Mediterranean forest stands. *Eur J Remote Sens.* **51**(1), 795–807. doi:10.1080/22797254.2018.1482733

12 Hackenberg J., Morhart C., Sheppard J., Spiecker H., Disney M., 2014. Highly accurate tree models derived from terrestrial laser scan data: a method description. *Forests*. **5**(5), 1069–1105. doi:10.3390/f5051069

13 Hackenberg J., Wassenberg M., Spiecker H., Sun D., 2015. Nondestructive method for biomass prediction combining TLS derived tree volume and wood density. *Forests.* **6**(4), 1274–1300. doi:10.3390/f6041274

14 Huang, H., Li, Z., Gong, P., Cheng, X., Clinton, N., Cao, C., *et al.* 2011 Automated methods for measuring DBH and tree heights with a commercial scanning Lidar. *Photogramm. Eng. Rem S.* **77**, 219–227. doi: 10.14358/PERS.77.3.219.

15 Kankare, V., Liang, X., Vastaranta, M., Yu, X., Holopainen, M. and Hyyppä, J., 2015 Diameter distribution estimation with laser scanning based multisource single tree inventory. *ISPRS J. Photogramm. Remote Sens.* **108**, 161–171. doi: 10.1016/j.isprsjprs.2015.07.007.

16 Kublin, E., 2003 Einheitliche Beschreibung der Schaftformmethoden und programme (uniform description of the stem volume functions and software)-bdatpro. *Forstwiss. Cent. Ver. Mit Thar. Forstl. Jahrb. 2003* **122**, 183–200.

17 Küng, O., Strecha, C., Beyeler, A., Zufferey, J.-C., Floreano, D., Fua, P., and Gervaix, F., 2011. The accuracy of automatic photogrammetric techniques on ultra-light UAV imagery. *Int. Arch. Photogramm. Remote Sens. Spatial Inf. Sci., XXXVIII-1/C22*, 125–130. doi: 10.5194/isprsarchives-XXXVIII-1-C22-125-2011.

18 Liang, X., Litkey, P., Hyyppa, J., Kaartinen, H., Vastaranta, M. and Holopainen, M., 2012 Automatic stem mapping using single-scan terrestrial laser scanning. *IEEE T. Geosci. Remote.* **50**, 661–670. doi: 10.1109/TGRS.2011.2161613.

19 Liang, X., Kankare, V., Yu, X., Hyyppa, J., Holopainen, M., 2014. Automated stem curve measurement using terrestrial laser scanning. *IEEE Trans Geosci Remote Sens.* **52**(3), 1739–1748. doi:10.1109/TGRS.2013.2253783

20 Liang, X., Wang, Y., Jaakkola, A., Kukko, A., Kaartinen, H., Hyyppa, J., *et al.* 2015 Forest data collection using terrestrial image-based point clouds from a handheld camera compared to terrestrial and personal laser scanning. *IEEE T. Geosci. Remote.* **53**, 5117–5132. doi: 10.1109/TGRS.2015.2417316.

21 Liang, X., Kankare, V., Hyyppä, J., Wang, Y., Kukko, A., Haggrén, H., *et al.* 2016 Terrestrial laser scanning in forest inventories. *ISPRS Photogramm. Remote Sens.* **115**, 63–77. doi: 10.1016/j.isprsjprs.2016.01.006.

22 Loetsch, F., Zoehrer, F., Haller, K.E. (1973). Forest Inventory. BLV, Munchen.

23 Lowe, D.G., 2004 Distinctive image features from scale-invariant keypoints. *Int. J. Comput. Vision.* **60**, 91–110. doi: 10.1023/B:VISI.0000029664.99615.94.

24 Maas, H.-G., Bienert, A., Scheller, S. and Keane, E., 2008 Automatic forest inventory parameter determination from terrestrial laser scanner data. *Int. J. Remote Sens.* **29**, 1579–1593. doi: 10.1080/01431160701736406.

25 Mikita, T., Janata, P. and Surový, P., 2016 Forest stand inventory based on combined aerial and terrestrial close-range photogrammetry. *Forests.* **7**, 165. doi: 10.3390/f7080165.

26 Miller, J., Morgenroth, J. and Gomez, C., 2015 3D modelling of individual trees using a handheld camera: accuracy of height, diameter and volume estimates. *Urban For. Urban Gree.* **14**, 932–940. doi: 10.1016/j.ufug.2015.09.001.

27 Mokroš, M., Liang, X., Surový, P., Valent, P., Čerňava, J., Chudý, F., *et al.* 2018. Evaluation of close-range photogrammetry image collection methods for estimating tree diameters. *ISPRS Int. J. Geoinf.* **7**(3), 93. doi:10.3390/ijgi7030093

28 Morgenroth, J. and Gomez, C., 2014 Assessment of tree structure using a 3D image analysis technique - a proof of concept. *Urban For. Urban Gree.* **13**, 198–203. doi: 10.1016/j.ufug.2013.10.005.

29 Moskal, L. M., & Zheng, G., 2011. Retrieving forest inventory variables with terrestrial laser scanning (TLS) in urban heterogeneous forest. *Remote Sens.* **4**(1), 1–20. doi:10.3390/rs4010001

30 Panagiotidis, D., Surový, P. and Kuželka, K., 2016 Accuracy of structure from motion models in comparison with terrestrial laser scanner for the analysis of DBH and height influence on error behaviour. *J. For. Sci.* **62**, 357–365. https://doi.org/10.17221/92/2015-JFS.

31 Patrone, G., 1963 *Lezioni di Dendrometria*. Accademia Italiana di Scienze Forestali, Firenze.

32 Piermattei, L., Karel, W., Wang, D., Wieser, M., Mokroš, M., Surový, P., *et al.* 2019. Terrestrial structure from motion photogrammetry for deriving forest inventory data. *Remote Sens*, **11**(8), 950.

33 Raumonen, P., Kaasalainen, M., Åkerblom, M., Kaasalainen, S., Kaartinen, H., Vastaranta, M., *et al.* 2013. Fast automatic precision tree models from terrestrial laser scanner data. *Remote Sens*, **5**(2), 491–520. doi:10.3390/rs5020491

34 Remondino, F., Fraser, C., 2006. Digital camera calibration methods: Considerations and comparisons. *Int. Arch. Photogramm. Remote Sens. Spatial Inf. Sci.* **36**(5), 266–272.

35 Remondino, F., Del Pizzo, S., Kersten, T.P. and Troisi, S., 2012 Low-cost and open-source solutions for automated image orientation—a critical overview. In *Progress in Cultural Heritage Preservation*. M., Ioannides, D., Fritsch, J., Leissner, R., Davies, F., Remondino, R., Caffo (eds.). Springer Berlin Heidelberg, pp. 40–54. doi: 10.1007/978-3-642-34234-9_5.

36 Srinivasan, S., Popescu, S.C., Eriksson, M., Sheridan, R.D. and Ku, N.W., 2014 Multi-temporal terrestrial laser scanning for modeling tree biomass change. *For Ecol Manage.* **318**, 304–317. doi: 10.1016/j.foreco.2014.01.038.

37 Stovall A.E.L., Shugart H.H., 2018. Improved biomass calibration and validation with terrestrial LiDAR: implications for future LiDAR and SAR missions. *IEEE J. Sel. Top. Appl.* **11**(10), 3527–3537. doi:10.1109/JSTARS.2018.2803110

38 Strahler, A.H., Jupp, D.L., Woodcock, C.E., Schaaf, C.B., Yao, T., Zhao, F., *et al.* 2008 Retrieval of forest structural parameters using a ground-based lidar instrument (Echidna ®). *Can. J. Remote Sens.* **34**, S426–S440. doi: 10.5589/m08-046.

39 Surový, P., Yoshimoto, A. and Panagiotidis, D., 2016 Accuracy of reconstruction of the tree stem surface using terrestrial close-range photogrammetry. *Remote Sens.* **8**, 123. doi: 10.3390/rs8020123.

40 Szeliski, R., 2011 *Computer vision. Algorithms and applications*. Springer.

41 Tarp-Johansen, M.J., Skovsgaard, J.P., Madsen, S.F., Johannsen, V.K. and Skovgaard, I., 1997 Compatible stem taper and stem volume functions for oak (Quercus Robur L and Q petraea (Matt) Liebl) in Denmark. *Annals of Forest Science* **54**, 577–595.

42 Ullman, S., 1979 The interpretation of structure from motion. *Proc. Roy. Soc. B-Biol. Sci.* **203**, 405–426. doi: 10.1098/rspb.1979.0006.

43 Van Aardt, J.A.N., Wynne, R.H. and Scrivani, J.A., 2008 Lidar-based mapping of Forest volume and biomass by taxonomic group using structurally homogenous segments. *Photogramm. Eng. Rem. S.* **74**, 1033–1044. doi: 10.14358/PERS.74.8.1033.

44 Verhoeven, G., Sevara, C., Karel, W., Ressl, C., Doneus, M. and Briese, C., 2013 Undistorting the past: new techniques for orthorectification of archaeological aerial frame imagery. In *Good Practice in Archaeological Diagnostics*. C., Corsi, B., Slapšak, F., Vermeulen (eds.), Springer International Publishing, pp. 31–67. doi: 10.1007/978-3-319-01784-6_3.

45 Wallace, L., Lucieer, A., Malenovský, Z., Turner, D. and Vopěnka, P., 2016 Assessment of Forest structure using two UAV techniques: a comparison of airborne laser scanning and structure from motion (SfM) point clouds. *Forests.* **7**, 62. doi: 10.3390/f7030062.

46 Wilkes, P., Lau, A., Disney, M., Calders, K., Burt, A., de Tanago, J.G., *et al.* 2017 Data acquisition considerations for terrestrial laser scanning of forest plots. *Remote Sens. Environ.* **196**, 140–153. doi: 10.1016/j.rse.2017.04.030.